Frequency-Reconfigurable MIMO Monopole Antenna with Wide-Continuous Tuning Range

Y. F. Cao*, S.W. Cheung, T.I. Yuk

Department of Electrical and Electronic Engineering, the University of Hong Kong, Pokfulam Road, Hong Kong
*yfcao@eee.hku.hk

Abstract: The design of a frequency-reconfigurable (FR) multiple-input-multiple-output (MIMO) monopole antenna with a wide-continuous tuning range in handheld devices is presented. The antenna consists of two symmetrical FR monopole elements and a FR defected-ground-structure (DGS). The monopole elements have two sections, sections 1 and 2, connected together using a PIN diode. Section 1 alone generates a high-frequency band at 2.26 GHz. By turning ON the PIN diode, sections 1 and 2 will be connected together to generate a low-frequency band at 1.93 GHz. The DGS is used to achieve high isolation between the monopole elements and is reconfigurable to follow the low- or high- frequency operations of the FR-MIMO antenna. Simple and novel biasing circuits employing only 3 DC wires are designed to control these diodes. The methodology of using the design in other frequency bands is proposed. Results on S-parameter, radiation pattern, realized peak gain and envelope-correlation coefficient (ECC) for pattern diversity are presented. Measured results show that the antenna has a wide-frequency tuning range from 1.88 to 2.64 GHz, covering the LTE 1, 2, 23, 25, 33-37 and 39-40 bands with low mutual-coupling and ECC of less than -20 dB and 0.5, respectively. The effects of the feeding cable used in measurement are also studied.

1. Introduction

Multiple-input-multiple-output (MIMO) technology has attracted much attention for its potential to increase the link quality and channel capacity of wireless systems without increasing the frequency spectrum [1]. Different MIMO antennas have been proposed for handheld devices in different communications systems such as the ultra-wideband (UWB) [2, 3], the global system for mobile communications (GSM) [4, 5], the long term evolution (LTE) [6, 7], and the wireless-local-area networks (WLANs) [8, 9]. With the developments of many different wireless communications standards, it is desirable to integrate as many standards as possible into a single wireless device. Multiband and wideband MIMO antenna have been proposed to serve this purpose [2-9]. However, frequency-reconfigurable (FR) MIMO antennas with the advantages of better out-of-band noise rejection [10] and more flexibility are more attractive to serve the same purpose. Different FR-MIMO antennas have been proposed such as those based on using monopole antennas [11-13], slot antennas [14], planar inverted-F antennas (PIFAs) [15] and loop antennas [16]. In [11-13], the FR of the MIMO monopole antennas were achieved by placing PIN diodes on the monopole elements to change the resonant frequencies. In [14], a FR MIMO slot antenna was designed by putting PIN diodes across the slot elements. In [15], a FR MIMO PIFA was designed by placing PIN diodes on both the planar inverted-F antenna (PIFA) radiators and the slits, so that the impedance bandwidth (IMBW) and isolation could be reconfigured simultaneously. In [16], a FR

MIMO loop antenna was proposed by changing the electrical length of the radiating loop using PIN diodes. The aforementioned MIMO antennas in [11-16] could only be tuned in discrete frequency bands and hence were limited to pre-designed applications. In applications such as the cognitive radio, continuous-frequency tuning of frequency band is needed. However, to the best knowledge of the authors, there has been little works focusing on continuous FR MIMO antennas.

In this paper, we propose the design of a FR MIMO monopole antenna with a wide-continuous tuning range for LTE handheld devices operating in the LTE 1-4, 9-10, 23, 25, 33-37 and 39-40 bands. The antenna mainly consists of two symmetrical FR monopole elements previously designed by the authors [17] and a FR defected ground structure (DGS). Each of the monopoles has two portions connected together using a PIN diode, with the operating frequency controlled using a varactor to achieve a wide tuning. By switching ON/OFF the PIN diodes on the monopoles and DGS, high isolation is achieved across the whole tuned-frequency band. A simple and novel biasing circuit employing only 3 DC wires is proposed to control all these six diodes. The FR MIMO monopole antenna has the advantages of wideband, continuous tuning, high isolation, and simple biasing circuit. The FR-MIMO antenna is designed and studied using the EM simulation tool CST. The effects of the feeding cable used in measurement on the antenna performance are also studied. A methodology is also proposed to design the FR-MIMO antenna.

2. Antenna design

2.1 Antenna Structure

The geometry of the proposed FR MIMO monopole antenna is shown in Fig. 1. The antenna consists of two symmetrical FR monopole elements and a symmetrical FR defected-ground structure (DGS), as shown in Figs. 1*a* and *b*. The design of the two monopole elements is obtained from the authors' previous design in [17] which is used here for MIMO antenna. The two antenna elements are individually fed using a microstrip line. The distance between these two elements is optimized to be $L3 = 0.1\lambda_g$ for mutual coupling of less than -20 dB for good performances [18-21], and smallest overall antenna size in the final design. Each monopole element has a compact overall size of $Wr \times Lr = 12.6 \times 8.7$ mm^2 with two sections, section 1 (having a meander shape) and section 2 (having a *U*-shape), which are connected together using a PIN diode (denoted as *D1* or *D1'* in Figs. 1*a*, *b* and *d*). With *D1* and *D1'* turned ON, denoted here as state I, both sections 1 and 2 of the monopole elements are electrically connected together, forming a longer radiator to generate a low-frequency band $B_{L,I}$ (where the scripts *L,I* denote the low frequency band in state I) at about 1.93 GHz. While with *D1* and *D1'* turned OFF, denoted here as state II, only sections 1 of the monopoles serve as the radiators and generate a high-frequency band $B_{L,II}$ at about 2.26 GHz. A varactor (denoted as *A1* or *A1'* in Figs. 1*a*, *b* and *d*) is placed on the radiator close to the microstrip feed-

line of each monopole element to tune the operating frequency band in the low-frequency range in state I and in the high-frequency range in state II. Applying a DC reverse-bias voltage *V1* across the varactors will reduce their capacitances and hence tune the frequency band to a higher frequency. The maximum reverse-bias voltage *V1* applied across the varactors will tune the frequency bands $B_{L,I}$ and $B_{L,II}$ in states I and II, respectively, to the corresponding highest frequency bands $B_{H,I}$ and $B_{H,II}$. To achieve a single and continuous-wide tuning range, sections 1 and 2 should be designed so that the highest tuned-frequency band $B_{H,I}$ in state I will be same as the lowest tuned-frequency $B_{L,II}$ in state II. The feed lines to the two monopole elements have a width of *Wf*=3.5 mm to achieve a characteristic impedance of 50 Ω.

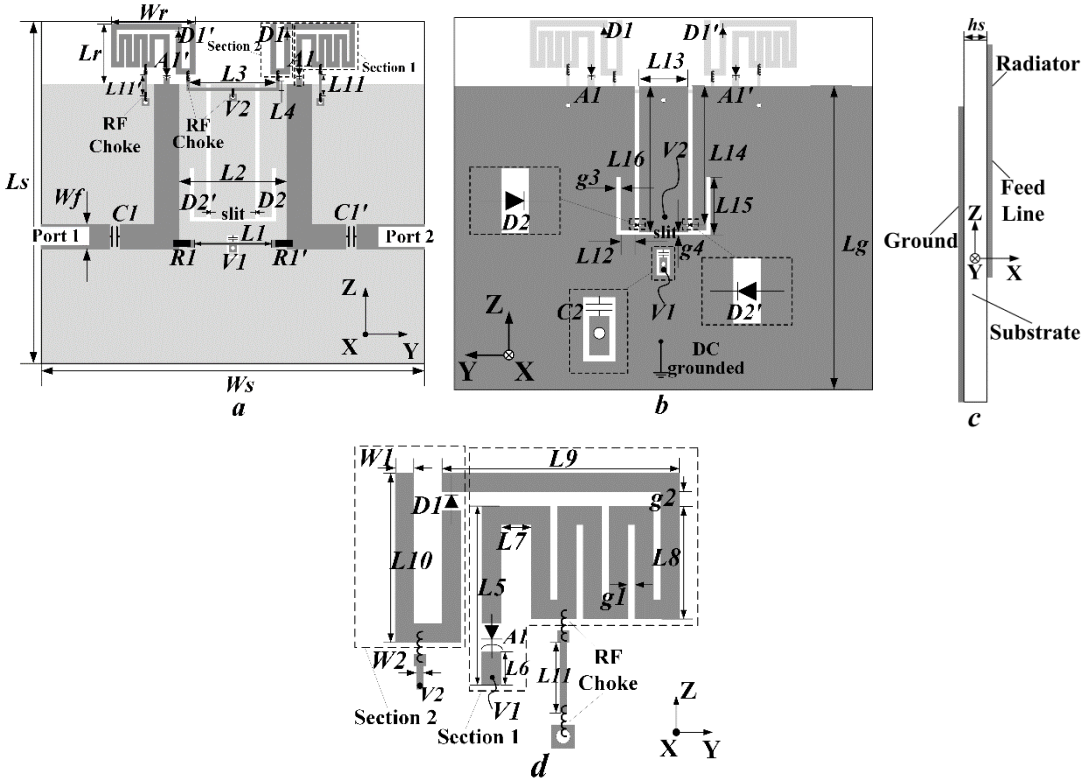

Fig. 1. *Geometry of antenna (dark color: metal in front and light color: metal in bottom)*
a top view
b bottom view
c side view
d radiator on right side

The FR DGS etched on the ground plane, as shown in Figs. 1*a* and *b*, is used to achieve good isolation between the two monopole elements. It has two symmetrically vertical *U*-shaped slots. The total length of each slot is designed to provide high isolation in the low-frequency tuning range in state I. A PIN diode (denoted as *D2* or *D2'* in Figs. 1*a* and *b*) is placed across each slot to control the electrical length. The locations of the PIN diodes on the slots are such that, when diodes *D2* and *D2'* are turned ON and short-circuited, the slot lengths are reduced to provide high isolation in the high-frequency tuning range in state II. In order to DC decouple the anodes from the cathodes of *D2* and *D2'* for biasing purpose, a thin

horizontal slit is etched on the ground plane to separate the DC potentials at the anodes and cathodes. Thus the center region of the DGS is also serving as a DC pad, which will be described in more details later.

In our design, just for a proof of concept, we have used the practical varactor, SMV 1405, SC-79, with a physical dimension of 1.2×0.7×0.5 mm^3, from Skyworks. In computer simulation, according to the data sheet [22], the varactor is modeled as a simple series circuit, consisting of a packaging parasitic inductance of Lf =0.7 nH, a series resistance of Rs =0.8 Ω, and a capacitance C_T ranging from 2.67 to 0.63 pF for the reverse voltage from 0 to 30 V. (According to the data sheet [22], the diode has a maximum reverse-bias voltage of 30 V. However, for safety reason in our study, we set the maximum voltage to only about 23.6 V.) For the PIN diodes, we have used BAR50-02V, SC-79, with a volume of 1.2×0.8×0.55 mm^3, from Infineon. According to the data sheet [23], the diode has a TURN-ON voltage of 0.95 V. In the "ON" state, the diode can be modeled using a forward resistance Rf = 3 Ω and a packaging parasitic inductance Lf= 0.6 nH connected in series for simulation. While in the "OFF" state, the circuit model can be modeled using a packaging parasitic inductance Lf= 0.6 nH in series with a parallel circuit having a capacitance Cp= 0.15 pF and a reverse resistance Rp= 5 kΩ.

The EM simulation tool CST is used to study and design the proposed FR MIMO antenna on a Rogers RO 4350 substrate with a relative permittivity of 3.66 and loss tangent of 0.004. The final dimensions of the antenna are listed in Table I and used to fabricate the prototype shown in Fig. 2 for measurement using the Satimo Starlab system.

TABLE 1 Dimensions of proposed antenna (mm)

L1	*L2*	*L3*	*L4*	*L5*	*L6*	*L7*	*L8*	*L9*	*L10*
11.1	15.5	12.6	1.6	7.3	1.2	1.3	4.5	10.6	7.5
L11	*L12*	*L13*	*L14*	*L15*	*L16*	*Lr*	*Lg*	*Ls*	*hs*
3.0	1.8	6.4	18.3	2.6	19.3	8.7	40.0	49.0	1.6
g1	*g2*	*g3*	*g4*	*Wf*	*Ws*	*W1*	*W2*	*Wr*	
0.35	0.6	0.6	0.3	3.5	55.0	0.8	0.3	12.6	

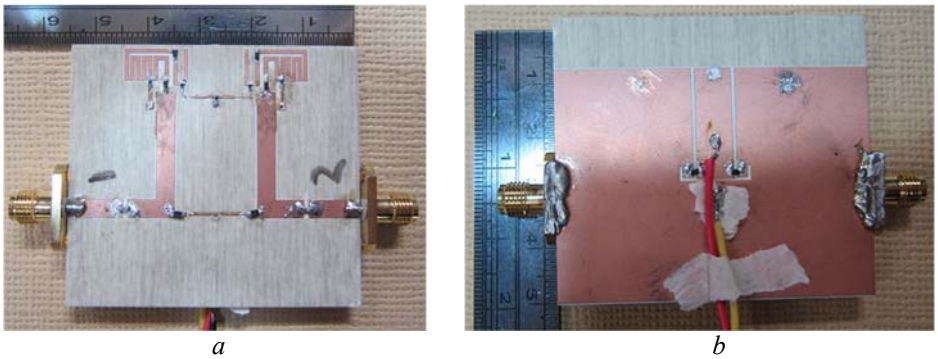

a *b*

Fig. 2. *Prototyped antenna (black wire for ground, yellow wire for controlling varactors and red wire for controlling PIN diodes)*
a top view; *b* bottom view

2.2 DC biasing circuits

There are four PIN diodes and two varactors used in the proposed FR-MIMO antenna of Fig. 1. It would be quite complicated to have six biasing circuits for these diodes. Here, we propose a simple biasing circuit requiring only two DC voltages to control the four PIN diodes (*D1, D1', D2* and *D2'*) and a simple biasing circuit to control the two varactors (*A1* and *A2*), as described as follows. In Fig. 1*a*, it can be seen that the anodes of varactors *A1* and *A1'* and cathodes of PIN diodes *D1* and *D1'* are connected to the antenna ground plane via the thin microstrip lines, *L11* and *L11'*, respectively. Here, antenna ground is also serving as common DC ground for biasing *A1, A1', D1* and *D1'*. Two RF chokes (inductors of 72 nH) are placed at both ends of the thin microstrip lines *L11* to prevent RF signals in the radiator from flowing through. The anodes of *D1* and *D1'* are connected to the center region of the DGS on the other side of the substrate through the thin microstrip line *L3,* a RF choke, a pad and a via. The RF choke is to further ensure no RF signal can get through. Thus the anodes of *D1* and *D1'* and the cathodes of *D2* and *D2'* are all DC connected to the center part of the DGS and have the same potential *V2*. The DC voltage *V2* is obtained through a (red) DC wire on the ground-plane side, as shown in Fig. 2*b*. All DC wires are placed on the ground-plane side to minimize the effects on the measured results.

Since the PIN diodes used in our design have a TURN-ON voltage of 0.95 V, applying *V2*=0.95V will turn ON *D1* and *D1'* to state I and connect sections 1 and 2 of the monopole elements together to form longer monopole elements, generating the low-frequency band $B_{L,I}$. At the same time, it will turn OFF *D2* and *D2'*, resulting in the longer slots in the DGS to provide high isolation in the whole low-frequency tuning range in state I of the antenna. When *V2*= -0.95 V is applied instead, *D1* and *D1'* will be turned OFF to state II to shorten the length of the monopole elements and generate the high-frequency band $B_{L,II}$. At the same time, *D2* and *D2'* will be turned ON to shorten the length of the slots on the DGS to provide high isolation in the whole high-frequency tuning range in state II of the antenna. Table II shows the DC voltages for states I and II of the antenna.

Table II DC voltages for states I and II of PIN diodes

	Voltage (V)	PIN diodes		Frequency range
	V2	*D1 & D1'*	*D2 & D2'*	
State I	0.95	ON	OFF	Low-frequency range
State II	-0.95	OFF	ON	High-frequency range

For biasing the varactors, it can be seen in Fig. 1*a* that the anodes of *A1* and *A1'* are connected to the DC ground plane, as previously described. A positive DC voltage of *V1* applied to microstrip line *L1* will reverse-bias *A1* and *A1'* and reduce their capacitances. This in turn shifts the operating band of the antenna to lower frequencies, making the antenna tunable. Two resistors *R1* & *R1'* (with 27 kΩ) are placed at both

ends of microstrip line *L1* and serving as chokes. The capacitors, *C1* and *C1'* (with 100 pF) in Fig. 1*a* are used as coupling capacitors to prevent DC biasing signals from getting into the signal input ports. DC signal *V1* on *L1* is obtained through a pad on the ground plane on the other side of the substrate and a via, as shown in Fig. 2*b*. Thus again, the DC wires are placed on the ground-plane side to minimize their effects on the measured results.

3. Studies of antenna

The geometry of the FR-MIMO antenna shown in Fig. 1 has many parameters such as *Lg*, *L1*-*L3*, *L5*-*L10*, *L12*-*L16*, *W1*, *W2*, and *g1*-*g3* which will affect the antenna performance. Here we try to find the parameters which can be used to set the low- and high-frequency bands and isolation independently, so that we can use the design for other applications. With the constraint of not increasing the total antenna size, simulation studies have shown that the four parameters *L8*, *L10*, *L14*, and *L15* can be used to set the operating frequency bands and so are used here for parametric study. In the parametric study, when port 1 is excited, port 2 is terminated with a 50-Ω load. In studying each parameter, the reverse-bias voltage is varied from 0 to 23.6 V to change C_T from 2.67 to 0.70 pF, respectively. However, to save page space, we only present here the results with C_T = 2.67 pF. Moreover, since the MIMO antenna has a symmetrical structure, S11 and S22 (the reflection coefficients seen by ports 1 & 2, respectively) should be the same, so we only present the simulated results for S11 and S21.

The simulated S11 and S21 in the parametric study in states I and II with C_T = 2.67 pF are shown in Figs. 3 and 4, respectively. Figs. 3*a* and 4*a* show that *L8* (the length of the meandered portion of section 1 shown in Fig. 1*d*) affects the resonant frequencies in both states, simply because *L8* determines the electrical length of the monopole elements. In state I, with *L8* increased from 3.5 mm to 4.5 and 5.5 mm, Fig. 3*a* shows that the low-frequency band $B_{L,I}$ (for S11 <-10 dB) shifts from 1.97-2.10 GHz to 1.87-1.98 and 1.78-1.88 GHz with mutual coupling (S21) increasing from about -24 dB to less than -21 dB and -19 dB, respectively. In state II, Fig. 4*a* shows that, for the same changes of *L8*, $B_{L,II}$ shifts from 2.28-2.61 GHz to 2.15-2.39 and 2.03-2.20 GHz with S21 less than -21 dB across the whole high-frequency tuning range. These results shows that *L8* can be used to set $B_{L,I}$ and $B_{L,II}$ in state I and II, respectively. Later on, in our proposed methodology of designing the antenna, and we use *L8* to set the $B_{L,II}$ in state II.

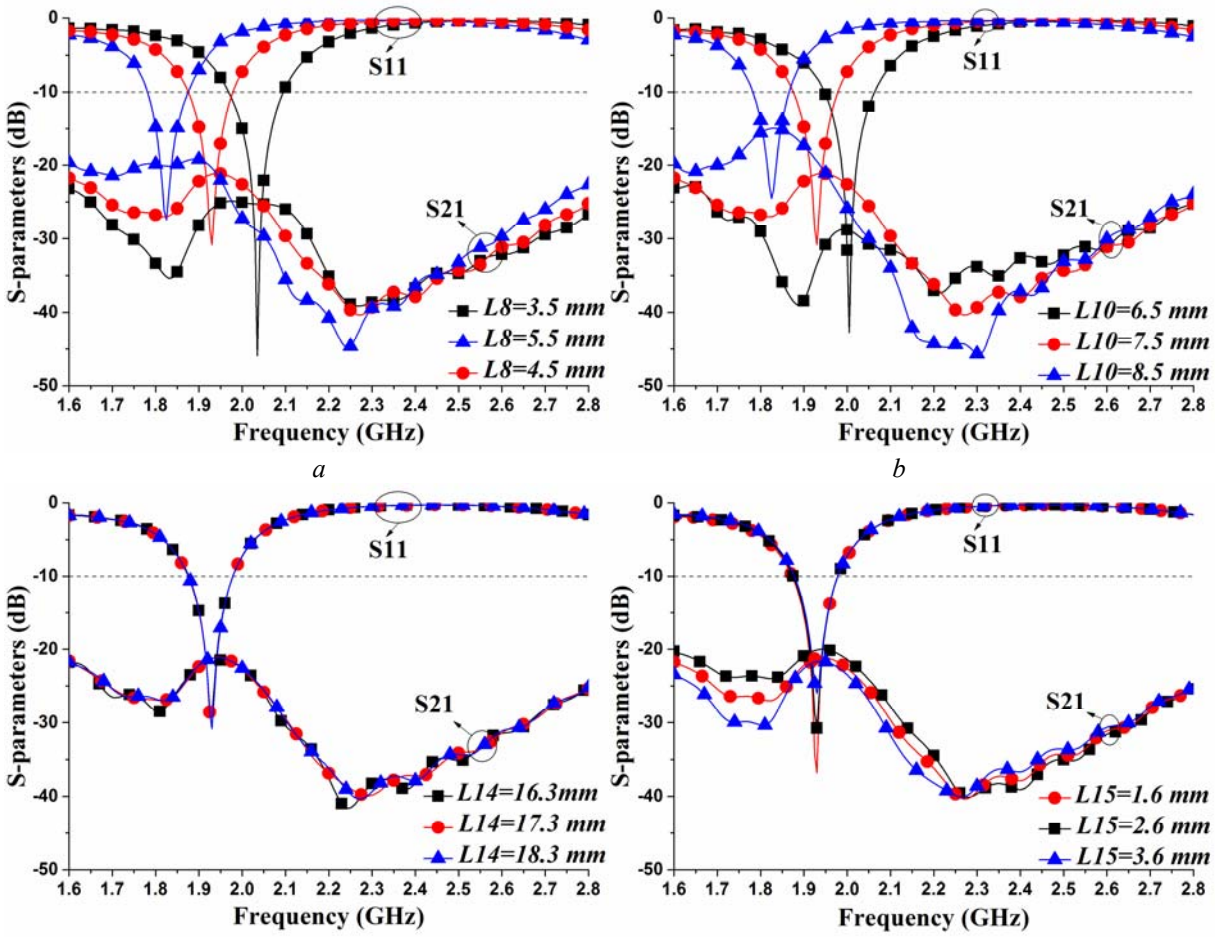

Fig. 3. *Simulated S11 and S21 with C_T = 2.35 pF in state I with different values of a L8;b L10;c L14;d L15*

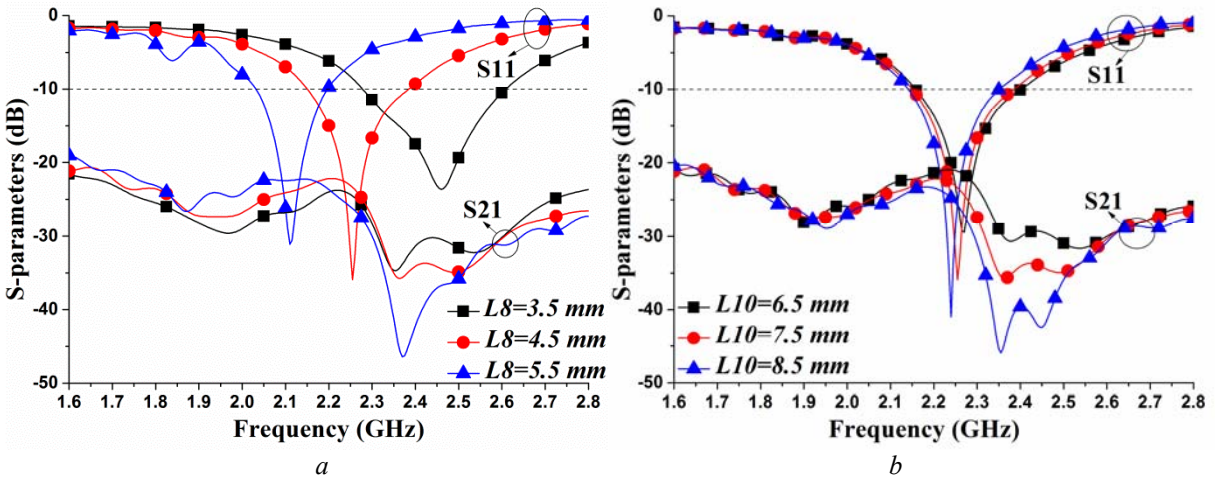

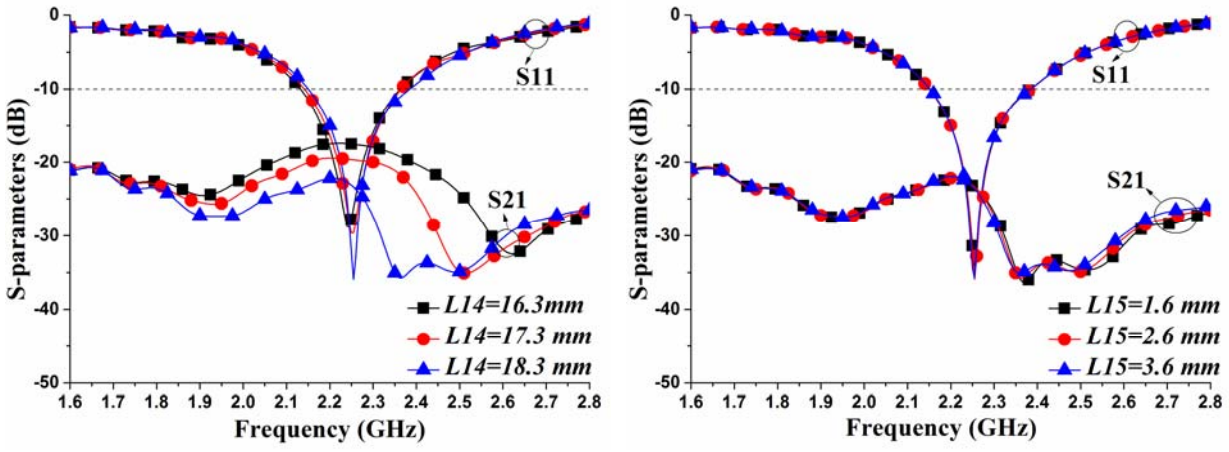

Fig. 4. *Simulated S11 and S21 with C_T = 2.35 pF in state II with different values a L8;b L10;c L14;d L15*

Figs. 3*b* and 4*b* show the effects of *L10* on S11 and S12 with C_T = 2.67 pF in states I and II, respectively. *L10* determines the length of the monopole elements in section 2 and is only effective in state I when *D1* and *D1'* are turned ON, so it should only affect $B_{L,I}$ in state I. Fig. 3*b* shows that, in state I, with *L10* increased from 6.5 mm to 7.5 and 8.5 mm, $B_{L,I}$ shifts from 1.95-2.06 GHz to 1.88-1.98 and 1.78-1.87 GHz, respectively, with S21 increasing from about -27 dB to less than -20 dB and then less than -14 dB. In state II, Fig. 4*b* shows that *L10* has little effects on the S11 and S21. Thus *L10* can be used to set $B_{L,I}$ in state I without affecting $B_{L,II}$.

The effects of *L14* on S11 and S21 in states I and II are shown in Figs. 3*c* and 4*c*, respectively. *L14* determines the locations of *D2* and *D2'* on the slots of the DGS, which affect isolation. In state I when *D2* and *D2'* are OFF, the locations of the diodes have no effect on the slot length, so Fig. 3*c* shows that *L14* has insignificant effects on S11 and S21 of the antenna. In state II when *D2* and *D2'* are ON, *L14* determines the slot lengths. As a result, Fig. 4*c* shows that, with *L14* increased from 16.3 mm to 17.3 and 18.3 mm, S21 changes from -17.5 dB to -19.6 and -23.1 dB, respectively, yet S11 remaining about the same. These results show that *L14* can be used to reduce S21 (mutual coupling) in state II without affecting S21 in state I.

The effects of *L15* on S11 and S21 in states I and II are shown in Figs. 3*d* and 4*d*, respectively. *L15* determines the overall slot lengths in the DGS when *D2* and *D2'* are OFF, and so only affects S21 (isolation) in state I. Fig. 3*d* shows that, in state I, increasing *L15* from 1.6 mm to 2.6 and 3.6 mm does not change the low-frequency band, but changes S21 from -20.0 dB to -21.0 and -22.0 dB, respectively, in the low-frequency band at about 1.93 GHz. In state II, Fig. 4*d* shows that increasing *L15* does not affect $B_{L,II}$ in terms of S11 and S21, so *L15* can be used to adjust S21 in state I independently without affecting $B_{L,II}$.

Simulation studies have been carried out on the effects of the DGS, with and without using the diodes, and with and without switching ON the diodes, on reducing coupling between the two antenna elements when the proposed RF MIMO antenna is operating in the frequency bands $B_{L,I}$, $B_{H,I}$, $B_{L,II}$, and

$B_{H,II}$. Results are shown in Fig. 5. Without using diodes *D2* and *D2'*, the simulated S21 with and without using the DGS are shown in Fig. 5*a*. It can be seen that the DGS can significantly reduce coupling in all $B_{H,II}$, $B_{L,II}$, $B_{H,I}$, and $B_{L,I}$. However, the coupling in $B_{H,II}$ are still above -20 dB which is not adequate for good performances [18-21], so *D2* and *D2'* are used on the DGS to further reduce the coupling in states I and II. When the antenna is operating in state II, i.e., *D2* and *D2'* are switched ON, Fig. 5*b* shows that the DGS can substantially reduce the coupling to less than -30 dB at the center frequencies of $B_{H,II}$ and $B_{L,II}$. When the antenna is operating in state I, i.e., *D2* and *D2'* are OFF, Fig. 5*c* shows that the DGS can reduce the coupling to less than -20 dB at the center frequencies of $B_{H,I}$ and $B_{L,I}$. Thus the DGS together with *D2* and *D2'* can reduce coupling to below -20 dB in the whole tuning frequency range.

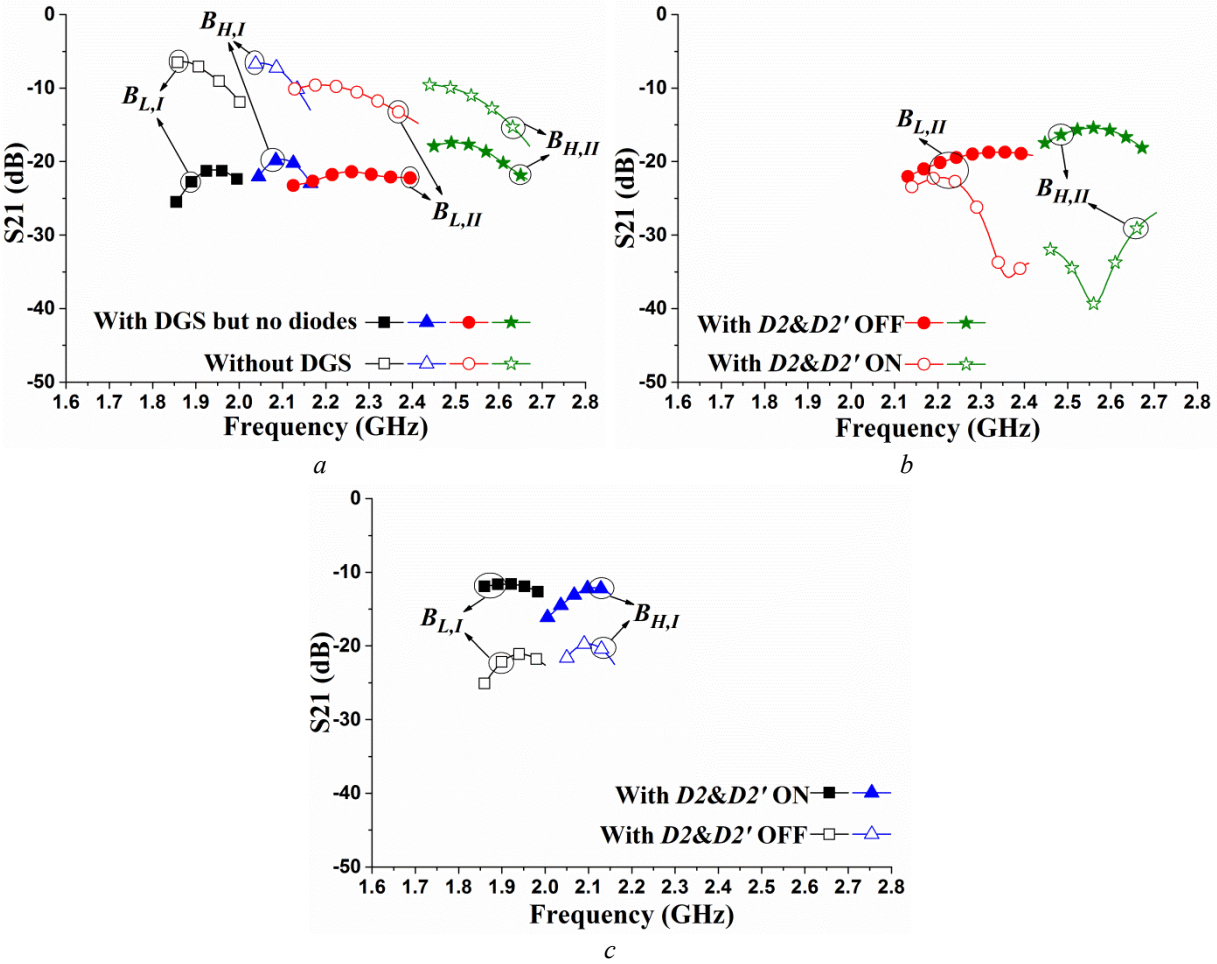

Fig. 5. *Simulated S21 of*
a MIMO antenna without DGS and with DGS but no diode
b Proposed MIMO antenna in state II with *D2* & *D2'* ON and OFF
c proposed MIMO antenna in state I with *D2* & *D2'* ON and OFF

Based on the above analysis, we attempt to propose a methodology to design the FR MIMO antenna with wideband, continuous tuning, and high isolation. Since the antenna employs 2 states to achieve a wide tuning range, we need to ensure continuity in tuning between states I and II. In our design methodology, we start with state II and then state I. In state II, we set the high frequency band $B_{H,II}$ and

then the low frequency band $B_{L,II}$. In state I, we set $B_{H,I}$ to be close to $B_{L,II}$ to ensure continuity in tuning between states I and II. Thus we propose the following method to design the FR-MIMO antenna:

In state II

1) Use *L8* with varactor capacitance $C_{T,min}$ (0.70 pF) to set $B_{H,II}$ in state II (see Fig. 4a).

2) Increase the varactor capacitance to $C_{T,max}$ (2.67 pF) to obtain $B_{L,II}$ in state II (see Fig. 3b).

In state I

3) Use *L10* with $C_{T,min}$ (0.7 pF) to set $B_{H,I}$ in state I to be close to $B_{L,II}$ in state II (this is to ensure continuous tuning from states I to II).

4) Increase the varactor capacitance to $C_{T,max}$ (2.67 pF) to obtain $B_{L,I}$ in state I (which is also the lowest frequency of the antenna).

5) Use *L14* to maximize isolation (S21) in the high-frequency tuning range of state II (see Fig. 4c)

6) Use *L15* to maximize isolation (S21) in the low-frequency tuning range of state I (see Fig. 3d)

The antenna is further studied using current distribution. With C_T = 2.67 pF and port 1 excited, the simulated current densities in states I and II at the center frequencies 1.93 GHz of $B_{L,I}$ and 2.26 GHz of $B_{L,II}$, respectively, are shown in Fig. 6. It can be seen in Figs. 6*a* and *b* that, with *D1* and *D1'* being ON and *D2* & *D2'* being OFF in state I, the currents concentrate on the whole lengths (sections 1 and 2 together) of the monopole elements, which contribute to resonance in the low-frequency tuning range. The currents also concentrate on the whole DGS. Figs. 6*c* and *d* show that, with *D1* and *D1'* being OFF and *D2* & *D2'* being ON in state II, the currents concentrate on section 1 of the monopole elements, which contribute to resonance in the high-frequency band. The current also concentrate on the vertical portion *L14* of the DGS. These observations agree with the results shown in Figs. 3 and 4.

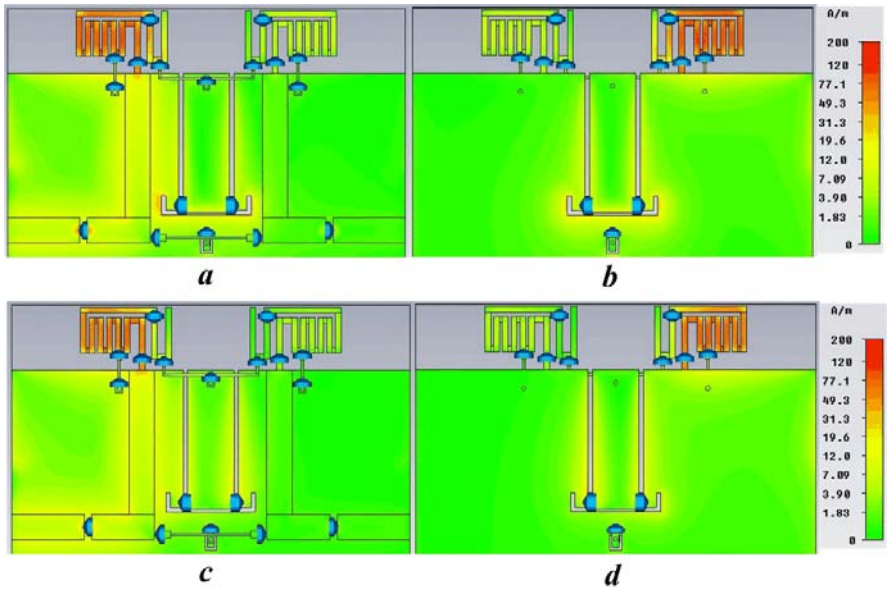

Fig. 6. *Simulated current distributions with C_T = 2.67 pF and port 1 excited*
a top view in state I at 1.93 GHz
b bottom view in state I at 1.93 GHz
c top view in state II at 2.26 GHz
d bottom view in state II at 2.26 GHz

4. Simulation and measurement results

The proposed FR-MIMO antenna of Fig. 1 has been studied using the EM simulation tool CST. For verification of simulation results, the prototyped antenna of Fig. 2 has been measured using the antenna measurement equipment, the Satimo Starlab system. In the studies, when one port is excited, the other one is terminated with a 50-Ω load.

4.1 Impedance bandwidth and isolation

The simulated and measured S-parameters of the proposed antenna in states I & II, using the maximum and minimum reverse-bias voltages leading to C_T =0.70 and 2.67 pF, respectively, have been studied. This means tuning from the lowest frequency to the highest frequency bands in both states I and II, i.e., tuning from $B_{L,I}$ to $B_{H,I}$ and then from $B_{L,II}$ to $B_{H,II}$. Results are shown in Fig. 7. Since the antenna has a symmetrical structure, the simulated S11 and S22 are identical as shown in Figs. 7*a* and *b*. The results show that the RF-MIMO antenna can be tuned from $B_{L,I}$ of 1.88-1.98 GHz to $B_{H,I}$ of 2.07-2.14 GHz in state I and then from $B_{L,II}$ of 2.15-2.39 GHz to $B_{H,II}$ of 2.47-2.64 GHz in state II. The antenna effectively can be tuned continuously from $B_{L,I}$ of 1.88-1.98 GHz to $B_{H,II}$ of 2.47-2.64 GHz, with the frequency tuning range from 1.88-2.64 GHz to cover the LTE 1, 2, 23, 25, 33-37 and 39-40 bands. Isolation in terms of S21 between the two input ports in these frequency bands is below -20 dB. Due to fabrication and measurement tolerances, the measured S11 and S22 in Figs. 7*a* and *b* are not exactly identical, but quite close to each other. So we take the average of S11 and S22 and compare it with the simulated S11 in Fig. 7*c*. It can be seen that the measured $B_{L,I}$, $B_{H,I}$, $B_{L,II}$ and $B_{H,II}$ are 1.83-1.99, 2.06-2.14, 2.14-2.45 and 2.53-2.66 GHz, respectively, indicating a continuous-frequency tuning range of 1.83 to 2.66 GHz, covering the LTE 1, 2, 23, 25, 33-37 and 39-40 bands. The discrepancies between the measured and simulated S11 and S21 in Fig. 7 are mainly due to the feeding cable used in measurement [24, 25], which can be described as follows. In computer simulation, no feeding cable is used. However, in measurements, a feeding cable is needed to connect the antenna to the measurement system (the Satimo Starlab system). At low frequencies, the ground plane of the antenna becomes electrically small and currents will flow back from the antenna to the outer surface of the feeding cable. This results in radiation causing inaccuracy in radiation patterns measurement, and also alters the current distribution on the antenna and hence the S11. To improve the accuracy in radiation pattern measurement, the feeding cable provided by Satimo for use in the Starlab system is covered with EM suppressant tubing to absorb unwanted radiation. However, because energy is absorbed, this method inevitably reduces the measured gain and efficiency of the antenna. To verify the effects of the feeding cable on the antenna performance, the cable model developed in [24, 25] is included in simulation and results are shown in Fig. 8. It can be seen that the simulated and measured S11 and S21 agree much better. Since feeding cable is not used in real applications, the performance of the FR-MIMO antenna should be closer to the simulated results.

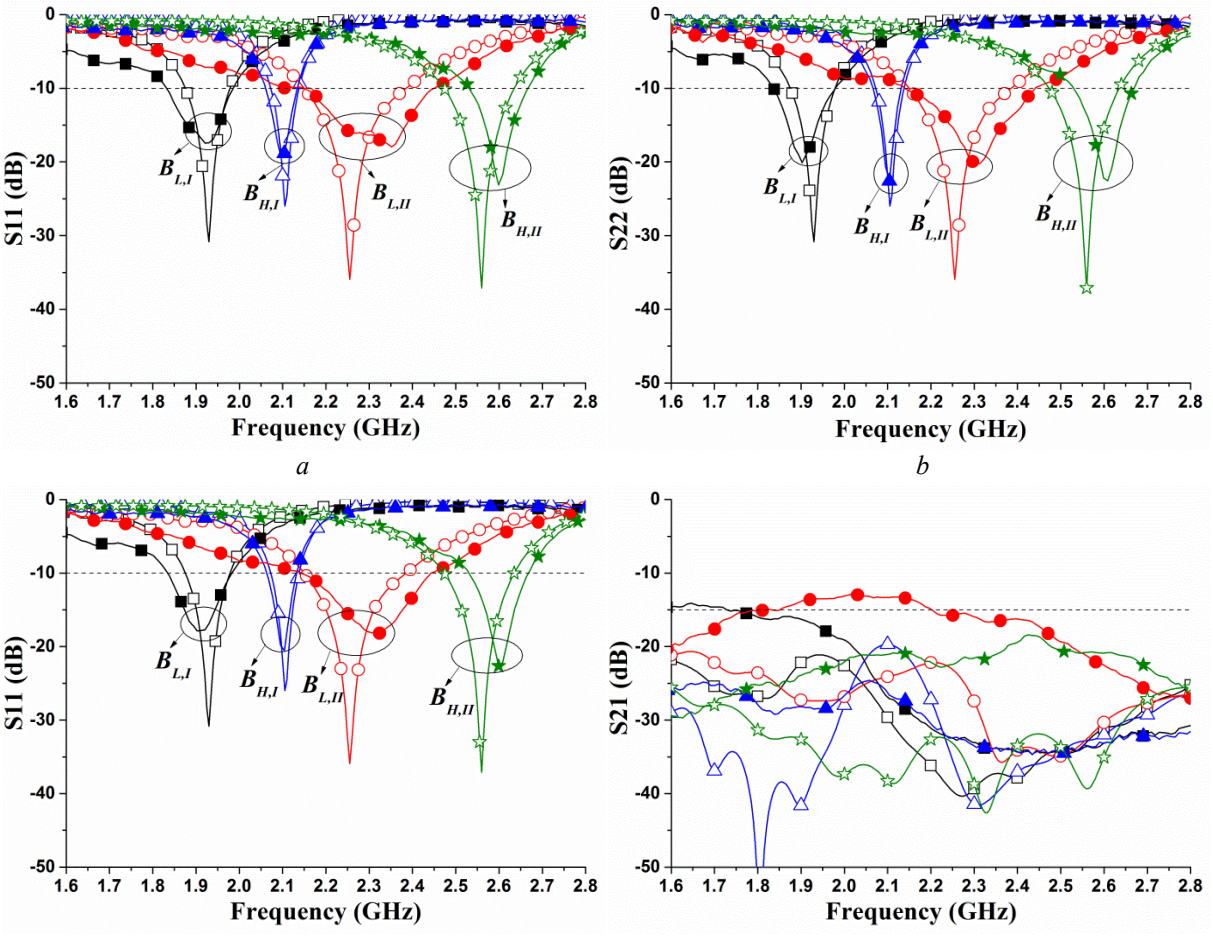

Fig. 7. *Measured and simulated results without cable model (simulation for* $B_{L,I}$ —□—, $B_{H,I}$ —△—, $B_{L,II}$ —○— *and* $B_{H,II}$ —☆—*; measurement for* $B_{L,I}$ —■—, $B_{H,I,}$ —▲—, $B_{L,II}$ —●—, *and* $B_{H,II}$ —★—*)*

a S11

b S22

c average of S11 & S22

d S21

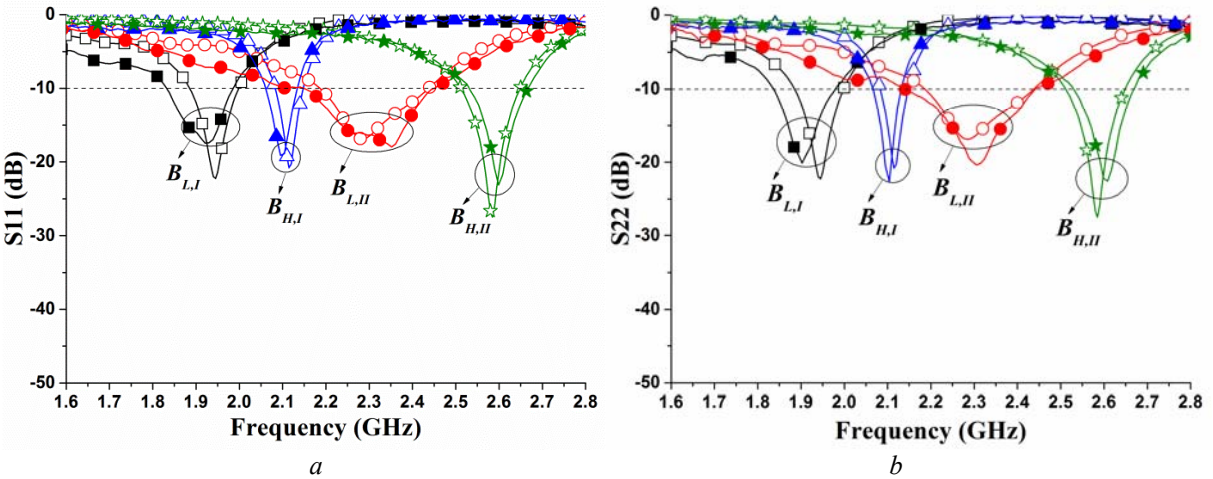

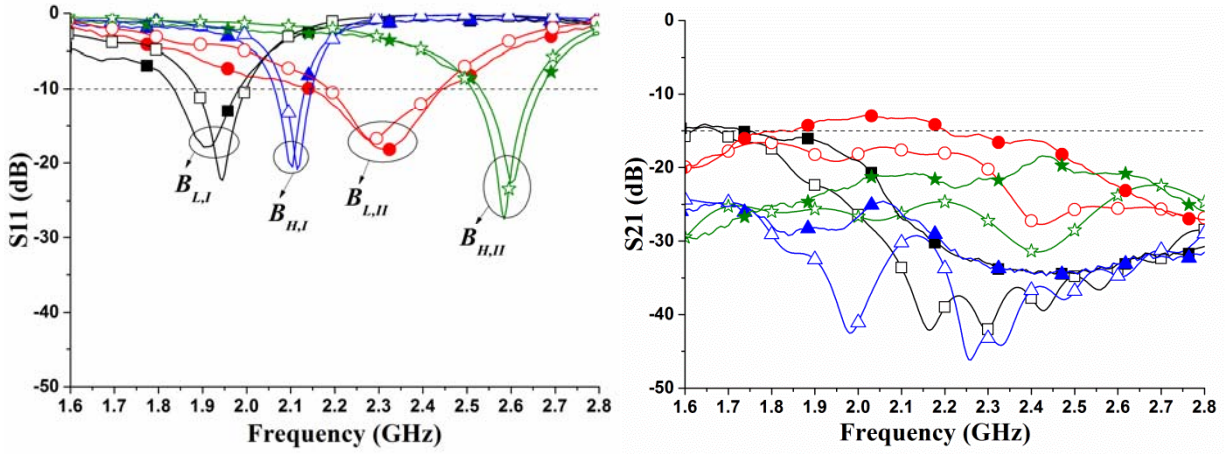

c *d*

Fig. 8. *Measured and simulated with cable model (simulation for $B_{L,I}$, $B_{H,I}$, $B_{L,II}$ and $B_{H,II}$; measurement for $B_{L,I}$, $B_{H,I}$, $B_{L,II}$, and $B_{H,II}$)*
a S11
b S22
c average of S11 & S22
d S21

4.2 Radiation Pattern

Simulation studies have shown that the FR-MIMO antenna has similar radiation patterns with different values of C_T in each state, so here we only show the simulated and measured results at 1.93 and 2.26 GHz which are the resonant frequencies in the lowest-frequency bands $B_{L,I}$ and $B_{L,II}$ in states I and II, respectively. At these frequencies, the FR-MIMO antenna has the simulated and measured S11 below –15 dB, as shown in Fig. 7*a*, and so should have similar radiated powers. The radiation patterns of the antenna with ports 1 or 2 excited at 1.93 and 2.26 GHz are shown in Fig. 9. It can be seen that the simulated and measured radiation patterns in the x-y plane are both omnidirectional, like conventional monopole. In the y-z plane, the radiation patterns are weaker on one side which is always covered by the patterns with the other port excited. This feature can be obviously seen in the 3D radiation patterns of Fig. 9. Thus the FR-MIMO antenna can be used for spatial pattern diversity. The simulated 2D radiation patterns using the cable model are also shown in Fig. 9 for comparison, indicating that the simulated 2D patterns using the cable model agree better with the measured results.

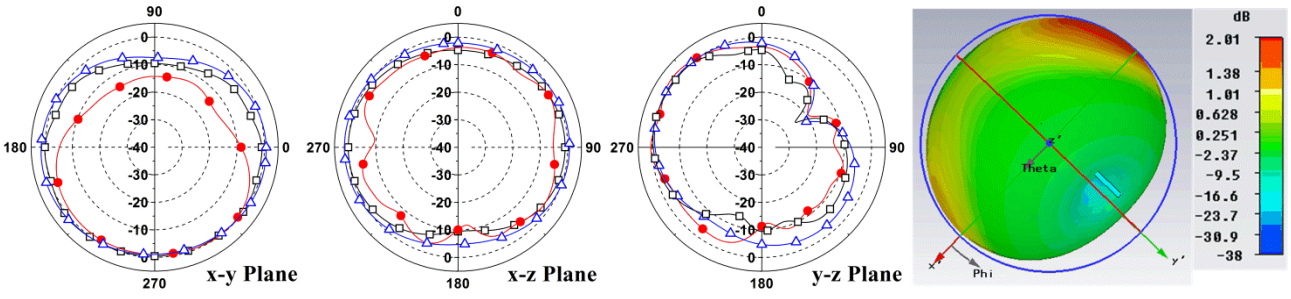

a

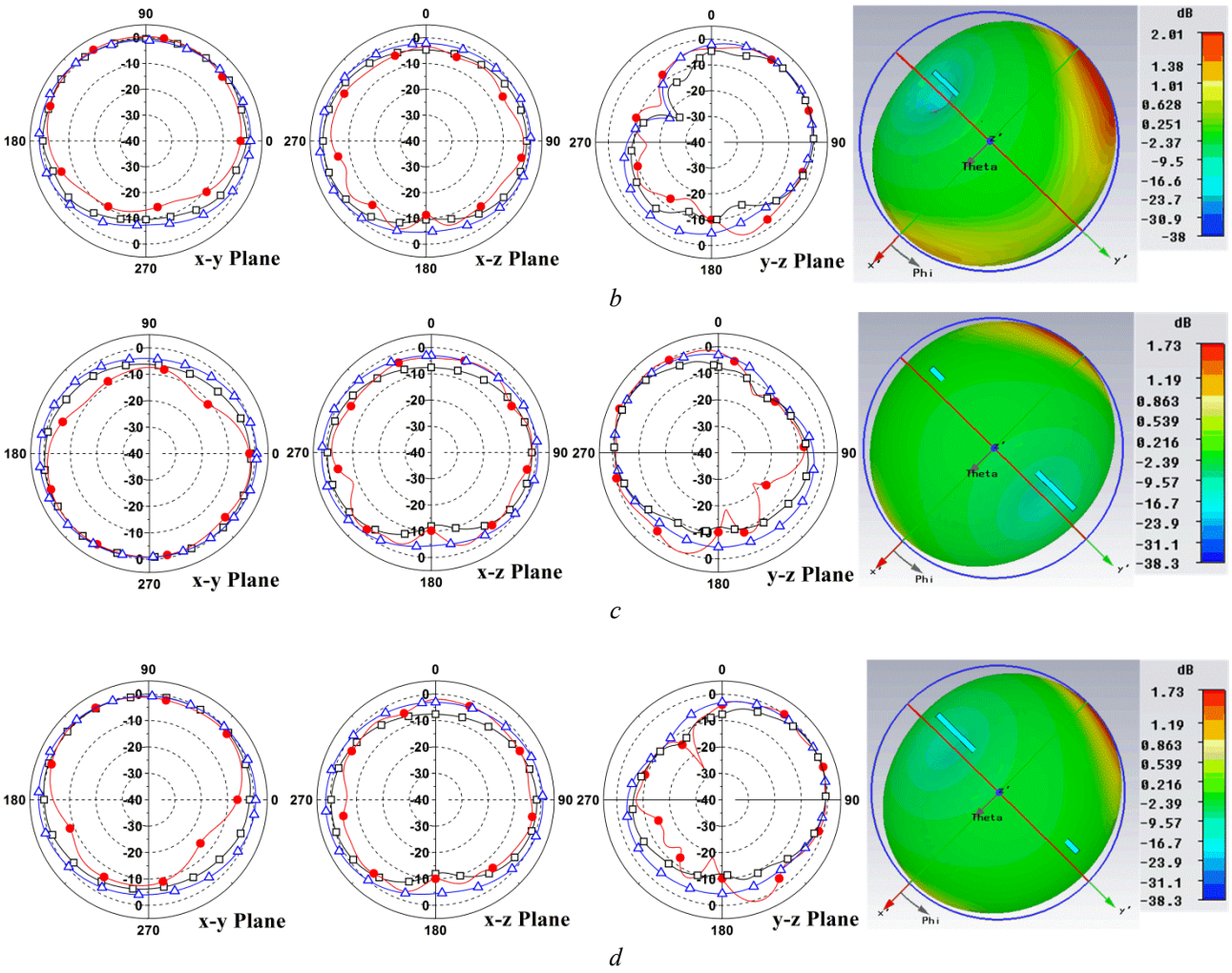

Fig. 9. *Simulated and measured radiation patterns (Simulation without cable model—△—, measurement—●—, and simulation with cable model—□—)*
a at 1.93 GHz in state I with port 1 excited
b at 1.93 GHz in state I with port 2 excited
c at 2.26 GHz in state II with port 1 excited
d at 2.26 GHz in state II with port 2 excited

4.3 Peak Gain

The simulated and measured results in realized-peak gain are shown in Figs. 10*a* and *b*. The simulated realized-peak gains at 1.93, 2.11, 2.26 and 2.56 GHz in the frequency bands of $B_{L,I}$, $B_{H,I}$, $B_{L,II}$ and $B_{H,II}$, respectively, are 1.79, 1.63, 1.85, and 1.98 dBi. When port 1 is excited, Fig. 10*a* shows that the measured realized-peak gains at 1.92, 2.10, 2.35 and 2.60 GHz in $B_{L,I}$, $B_{H,I}$, $B_{L,II}$ and $B_{H,II}$, respectively, are 0.83, -0.11, 0.94, and 1.22 dBi. While when port 2 is excited, Fig. 10*b* shows that the measured realized-peak gains for these frequency bands at 1.90, 2.10, 2.31 and 2.61 GHz are 0.93, 0.07, 0.69 and 1.12 dBi, respectively. The simulated and measured results agree well.

4.4 Diversity Performance

The envelope-correlation coefficient (ECC) ρ_e for evaluating the correlation between radiation patterns of the two radiators is calculated using the 3-D radiation patterns as [15, 26]

$$\rho_e \approx \left|\rho_c\right|^2 \tag{1}$$

where ρ_c is the complex-correlation coefficient given by

$$\rho_c = \frac{\int_0^{2\pi} M_{12}(\phi)d\phi}{\sqrt{\int_0^{2\pi} M_{11}(\phi)d\phi \int_0^{2\pi} M_{22}(\phi)d\phi}} \tag{2}$$

with

$$M_{ij}(\phi) = \Gamma E_{\theta i}(\pi/2,\phi)E^*_{\theta j}(\pi/2,\phi) + E_{\phi i}(\pi/2,\phi)E^*_{\phi j}(\pi/2,\phi) \tag{3}$$

In (3), $\vec{E}_i(\theta,\phi) = E_{\theta i}(\theta,\phi)\hat{\theta} + E_{\phi i}(\theta,\phi)\hat{\phi}$ is the vector radiation pattern of the *i*-th antenna, Γ is the cross-polarization power ratio of the incident wave, and '*' denotes the complex conjugate. With the use of (2) and (3), the ECC at the corresponding resonance frequencies for frequency bands $B_{L,I}$, $B_{H,I}$, $B_{L,II}$ and $B_{H,II}$ (for S11< -10 dB) using the measured and simulated radiation patterns without using the cable model are shown in Fig. 10*c*. It can be seen that the ECCs using the simulated radiation patterns in all frequency bands are very close to zero value, while the ECCs using the measured radiation patterns are less than 0.5. Note that a MIMO antenna with an ECC of less than 0.5 can achieve a good diversity performance [27]. Thus the results in Fig. 10*c* show that the proposed FR MIMO antenna achieves a good diversity gain across the whole tuning range.

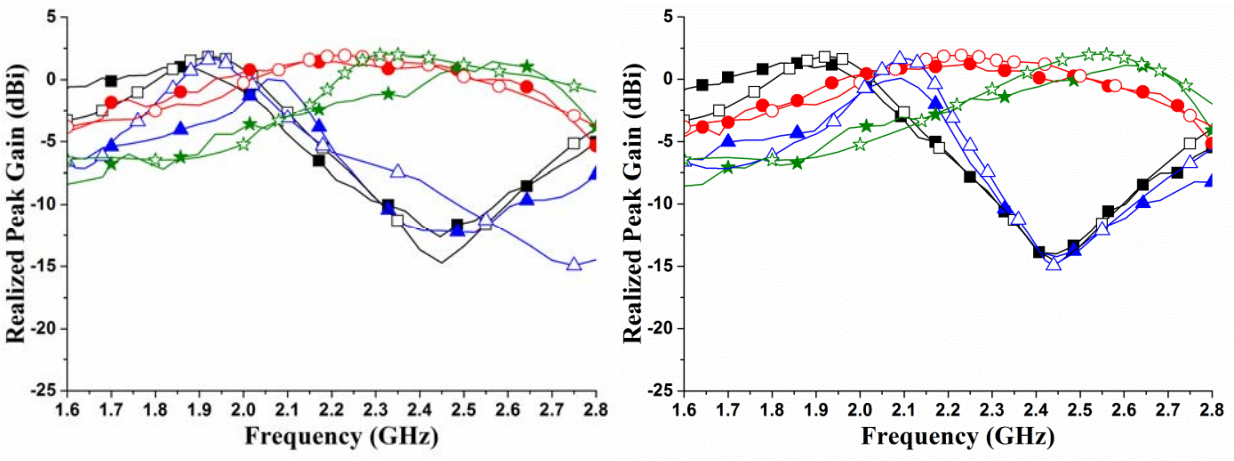

a *b*

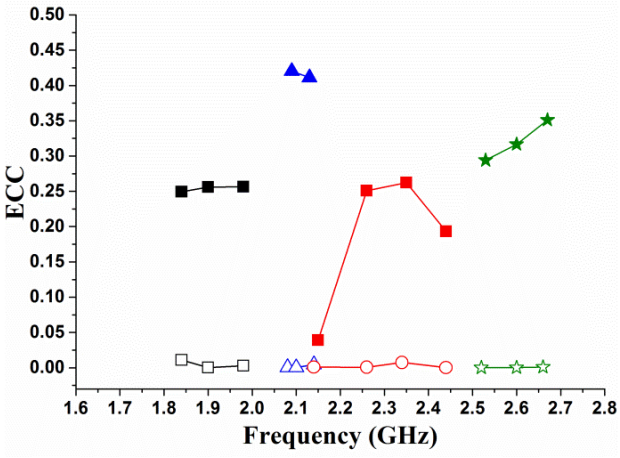

c

Fig. 10. *Simulated and measured realized peak gains and ECC (simulation for $B_{L,I}$, $B_{H,I}$, $B_{L,II}$ and $B_{H,II}$; measurement for $B_{L,I}$, $B_{H,I,}$, $B_{L,II}$, and $B_{H,II}$)*
a realized peak gains with port 1 excited
b realized peak gains with port 2 excited
c ECC

4.5 Performance comparison with previous works

The size, mode of switching, covering bands, isolation and gain of the proposed MIMO antenna are compared with those of previous works [12-16] in Table III. It can be seen that the size of the proposed MIMO antenna is the smallest among others, except the one in [13] which however has narrower operating frequency bands and lower isolation. Since the previous works in [12-16] support switching between discrete operating bands which are not continuous, while our proposed antenna supports continuous tuning with a wide tuning range, it is difficult to compare their tuning ranges. In Table III, we use covering bandwidth in % for comparison. It can be seen that the proposed antenna has the largest covering bandwidth of 32.2% and highest isolation of 22 dB among all, except the one in [15] which however has a much smaller tuning range. Thus the proposed antenna has a better overall performance. One major drawback of the antenna is low gain which needs to be improved and is our future work.

Table III Comparison of proposed antenna with previous works

	Total Size (λ_g^2)	Switching Mode (total covering bandwidth)	State	Covering bands (GHz)	Isolation (dB)	Gain (dBi)
[12]	1.05×0.53=0.5565	Discrete (26%)	I	3.18-3.72 (15.7%)	>13	5.28
			II	2.4-2.5 (4.1%)	>21	4.54
				5.15-5.48 (6.2%)	> 23	3.92
[13]	0.66×0.29=0.1914	Discrete (24%)	I	2.44- 2.8 (13.7%)	> 12	-
			II	5.05-5.6 (10.3%)	> 15	-
[14]	0.64×0.51=0.3264	Discrete (9.3%)	I	0.82-0.86 (4.8%)	>3	-
			II	1.08-1.13 (4.5%)	>6	-
[15]	0.66×1.19=0.7854	Discrete (13.4%)	I	3.4-3.6 (5.7%)	> 30.8	2.78
			II	2.5-2.7 (7.7%)	> 43	1.99
			III	2.3-2.4 (4.3%)	> 47	1.39
[16]	1.33×1.33=1.7689	Discrete (20.8%)	I	1.71-1.88 (9.5%)	> 9	3-5.2
			II	2.50-2.80 (11.3%)	> 10	5.5
Pro	0.50×0.45=0.2250	Continuous (32.4%)	I & II	1.81-2.51 (32.4%)	> 22	1.4

5. Conclusions

The design of a FR MIMO antenna with a wide-continuous tuning range has been presented. The antenna consists of two symmetrical FR monopole elements and a symmetrical FR DGS. The monopole elements have two sections connected together using a PIN diode. Tuning operating is accomplished using varactors. The DGS for isolation is also reconfigurable to follow the low- and high- operating bands. Simple and novel biasing circuits employing only 3 DC wires have been proposed to control the diodes. The methodology of using the design in other frequency bands has been proposed. Measured results show that the antenna has a wide-frequency tuning range from 1.88 to 2.64 GHz, covering the LTE 1, 2, 23, 25, 33-37 and 39-40 bands with low mutual-coupling and ECC of less than -20 dB and 0.5, respectively. The effects of the feeding cable used in measurement are also studied.

6. References

[1] Zheng, L., Tse, C.: 'Diversity and multiplexing: a fundamental tradeoff in multiple-antenna channels', IEEE Trans. Inf. Theory., 2003, **49**, pp. 1073-1096

[2] Zhang, S., Lau, B. K., Sunesson, A., He, S.: 'Closely-packed UWB MIMO/diversity antenna with different patterns and polarizations for USB dongle applications', IEEE Trans. Antennas Propag., 2012, **60**, (9), pp. 4372–4380

[3] Liu, L., Cheung, S. W., Yuk, T. I.: 'Compact MIMO antenna for portable devices in UWB applications', IEEE Trans. Antennas Propag., 2013, **61**, (8), pp. 4257-4264

[4] Zhou, X., Quan, X. L., Li, R. L.: 'A dual-broadband MIMO antenna system for GSM/UMTS/LTE and WLAN handsets', IEEE Antennas Wireless Propag. Lett., 2012, **11**, pp. 551-554

[5] Wang, Y., Du, Z. W.: 'A printed dual-antenna system operating in the GSM1800/GSM1900/UMTS/LTE2300/LTE2500/2.4-GHz WLAN bands for mobile terminals', IEEE Antennas Wireless Propag. Lett., 2014, **13**, pp. 233-236

[6] Ren, Y. J.: 'Ceramic based small LTE MIMO handset antenna', IEEE Trans. Antennas Propag., 2013, **61**, (2), pp. 934-938

[7] Lee, B., Harackiewicz, F. J., Wi, H.: 'Closely mounted mobile handset MIMO antenna for LTE 13 band application', IEEE Antennas Wireless Propag. Lett., 2014, **13**, pp. 411-414

[8] Liao, W. J., Chang, S. H., Yeh, J. T., Hsiao, B. R.: 'Compact dual-band WLAN diversity antennas on USB dongle platform', IEEE Trans. Antennas Propag., 2014, **62**, (1), pp. 109-118

[9] Su, S. W., and Lee, C. T.: 'Low-cost dual-loop-antenna system for dual-WLAN-band access points', IEEE Trans. Antennas Propag., 2011, **59**, (5), pp. 1652-1659

[10] Yang, S., Zhang, C., Pan, H., Fathy, A., Nair, V.: 'Frequency-reconfigurable antennas for multiradio wireless platforms', IEEE Microw. Mag., 2009, **10**, (1), pp. 66–83

[11] Ghasemi, A., Ghahvehchian, N., Mallahzadeh, A., Sheikholvaezin, S.: 'A reconfigurable printed monopole antenna for MIMO application'. 6th European Conference on Antennas and Propagation (EUCAP), Prague, Czech, 2012, pp.1-4

[12] Jin, Z. J., Lim, J. H., Yun, T. Y.: 'Frequency reconfigurable multiple-input multiple output antenna with high isolation', IET Microw. Antennas Propag., 2012, **6**, (10), pp. 1095-1101

[13] Luo, R. Q., Pereira, J. R., Salgado, H. M.: 'Reconfigurable dual-band C-shaped monopole antenna array with high isolation', Electron Lett., 2010, **46**, (13), pp. 888-889

[14] Yan, J. B., Yong, S., Bernhard, J. T.: 'Intermodulation and harmonic distortion in frequency reconfigurable slot antenna pairs', IEEE Trans. Antennas Propag., 2014, **62**, (3), pp. 1138-1146

[15] Lim, J. H., Jin, Z. J., Song, C. W., Yun, T. Y.: 'Simultaneous frequency and isolation reconfigurable MIMO PIFA using PIN diodes', IEEE Trans. Antennas Propag., 2012, **60**, (12), pp. 5939-5946

[16] Kulkarni, A. N., Sharma, S. K.: 'Frequency reconfigurable microstrip loop antenna covering LTE bands with MIMO implementation and wideband microstrip slot antenna all for portable wireless DTV media player', IEEE Trans. Antennas Propag., 2013, **61**, (2), pp. 964-968

[17] Cao, Y. F., Cheung, S. W., Sun, X. L., Yuk, T. I.: 'Frequency-reconfigurable monopole antenna with wide tuning range for cognitive radio', Microw. Opt. Tech. Lett., 2014, **56**, (1), pp. 145-152

[18] T. K. Roshna, U. Deepak, V. R. Sajitha, K. Vasudevan, and P. Mohanan, "A compact UWB MIMO antenna with reflector to enhance isolation," IEEE Trans. Antennas Propag., 2015, **63**, (4), pp. 1873-1877

[19] M. A. Abdalla and A. A. Ibrahim, "Compact and closely spaced metamaterial MIMO antenna with high isolation for wireless applications," IEEE Antennas Wireless Propag. Lett., 2013, **12**, pp. 1452-1455

[20] H. Wang, Z. J. Zhang and Z. H. Feng, "Dual-port planar MIMO antenna with ultra-high isolation and orthogonal radiation patterns," Electron Lett., 2015, **51**, (1), pp. 7-8

[21] C. X. Mao, Q. X. Chu, Y. T. Wu, and Y. H. Qian, "Design and investigation of closely-packed diversity UWB slot-antenna with high isolation," Progress In Electromagnetics Research, 2013, **41**, pp. 13-25

[22] SMV1405 to SMV1430 Series: Plastic Packaged Abrupt Junction Tuning Varactors, Skyworks Solutions, Inc., USA, Jan. 25,, 2016.

[23] Datasheet for bar50series, Infineon Technologies AG81726 Munich, Germany, Jul 2011.

[24] Liu, L., Weng, Y. F., Cheung, S. W., Yuk, T. I., Foged, L. J.: 'Modeling of cable for measurements of small monopole antennas', Loughborough Antennas & Propagation Conference, Loughborough, UK, 2011, pp. 1-4

[25] Liu, L., Cheung, S. W., Weng, Y. F., Yuk, T. I.: 'Cable effects on measuring small planar UWB monopole antennas' in "Ultra Wideband", Edited by Mohammad Matin, Intech, ISBN 978-953-51-0781-1, Oct. 2012.

[26] Knudsen, M. B., Pedersen, G. F.: 'Spherical outdoor to indoor power spectrum model at the mobile terminal', IEEE J. Sel. Areas Commun., 2002, **20**, (6), pp. 1156-1168

[27] Vaughan, R. G., Andersen, J. B.: 'Antenna diversity in mobile communications', IEEE Trans. Veh. Tech., 1987, **36**, (4), pp. 149-172